Chapter 6

Extending surface hopping

FOB-SH is a variant of Tully's original fewest switches surface hopping[105]. It has been used to simulate electron-nuclear dynamics in large systems of organic molecules and has been well tested against experimental studies and benchmarked against higher order studies[14,69–76]. However, the code does not currently account for any electrostatic interactions. This presents a problem when looking at many systems; such as those with large amounts of disorder or those with polariseable molecules.

The standard Coulomb sum of partial charges is only conditionally convergent and extremely slow to calculate. The standard method for calculating electrostatic interactions is by decomposing interactions into long-range and short-range interactions (with corrections such as removing bonded terms etc…). This is normally carried out with an Ewald sum[106] where a short-range interactions are calculated in real-space and long-range interactions are calculated in reciprocal-space. This results in 2 summations that are now unconditionally, quickly convergent. Further extensions to the standard Ewald technique provide an additional decrease in computational time by interpolating particles onto a grid and using fast fourier transforms to calculate the sums. In Wolf, 99[107], a technique for removing the (expensive) reciprocal-space term from the sum altogether was proposed by ensuring charge neutrality within a cutoff sphere from each atom. This idea was developed to improve energy conservation and to remove discontinuities within the forces and energies[108,109]. In this work I will investigate the applicability of both the standard Ewald technique and a development of the Wolf method (named DSF[109]) to calculate

the electrostatic interactions within FOB-SH.

6.1 Implementation details

6.1.1 Addition Subtraction Method

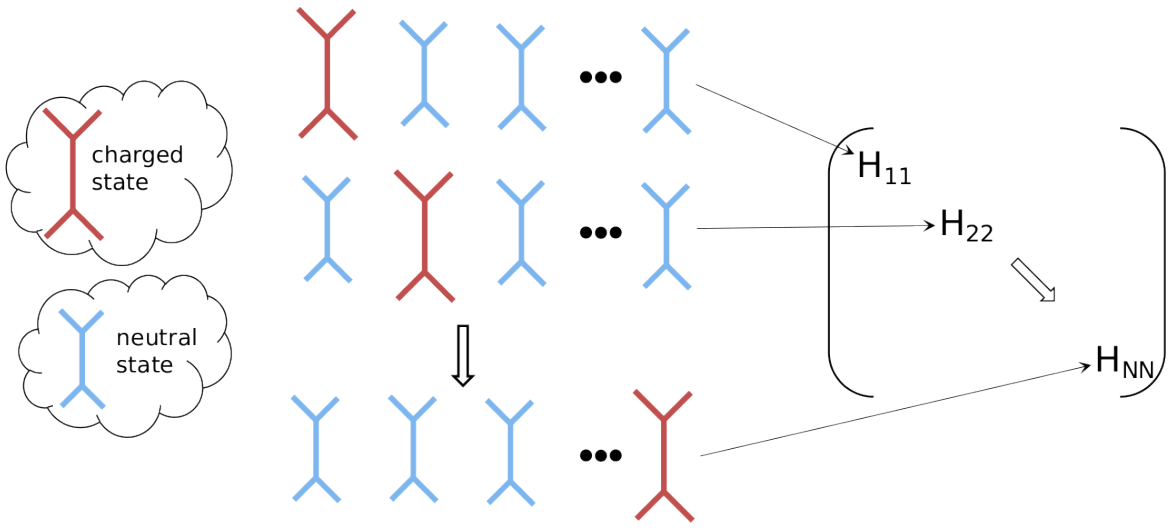

Figure 6.1: A demonstration of the procedure to calculate diagonal elements of the Hamiltonian (site-energies). Red (blue) shapes represent a molecule in it's charged (neutral) state. A horizontal line of these shapes represent the full system with all molecules; where a single molecule is in it's charged state. The arrow denotes which matrix element this saved as.

In FOB-SH, nuclear dynamics are determined by the Hamiltonian. The Hamiltonian is constructed such that the diagonal elements (site-energies) come from a classical forcefield and the off-diagonal elements (electron couplings) are proportional to the overlap of the diabatic wavefunctions. Each site-energy, $H_{\gamma\gamma}$, is defined as the potential energy of the system where the excess charge is localised on the molecule γ. For the avoidance of doubt, I will denote the molecule with the excess charge localised on it as the 'charged' molecule and other molecules as 'neutral'. The presence of the excess charge on molecule γ results in different input parameters (such as the charge distribution or the length of bonds) than the other neutral molecules. This results in the calculation of site-energies and forces having to be repeated N_{mol} times for each permutation of the charged molecule. This is

summarised in figure 6.1.

To determine whether it is feasible to repeat the calculation of the electrostatic interactions N_{mol} times a quick timing run was carried out. This simulated 250 pentacene molecules (9,000 atoms) and the time was measured to calculate the electrostatic interactions with the 3 methods already implemented within CP2K: Smooth Particle Mesh Ewald (SPME), Particle Mesh Ewald (PME) and standard Ewald. The measured time of a simulation without any electrostatics was then subtracted from each of these simulations to isolate the time spent on just the electrostatics. The results are given in figure 6.2.

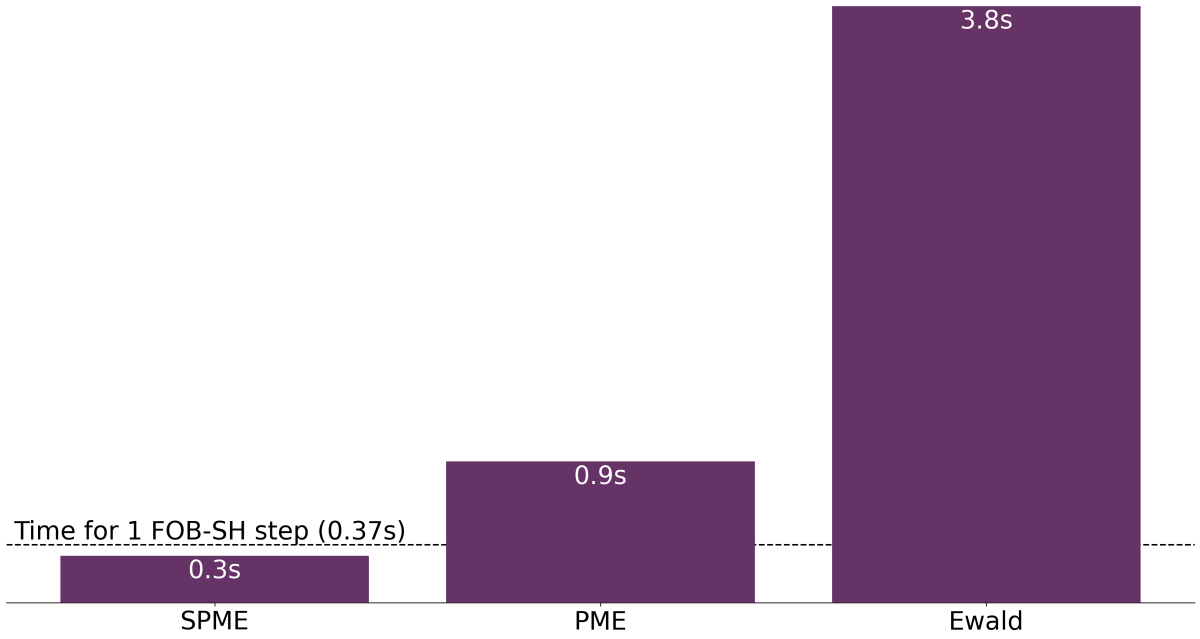

Figure 6.2: The time taken to calculate just the electrostatic interactions within CP2K for a 9,000 atom system using various methods. PME is particle mesh Ewald, SPME is smooth-PME, Ewald is the standard ewald method. The dashed line shows the time taken for a single FOB-SH step.

We can see that even a single calculation of the electrostatic interactions with the fastest method available within CP2K will take a comparable time to the rest of the surface hopping code. It is clear then that a more efficient method must be used to calculate the electrostatics in a more efficient way.

Within the current FOB-SH implementation the forces and energies consist of intra-

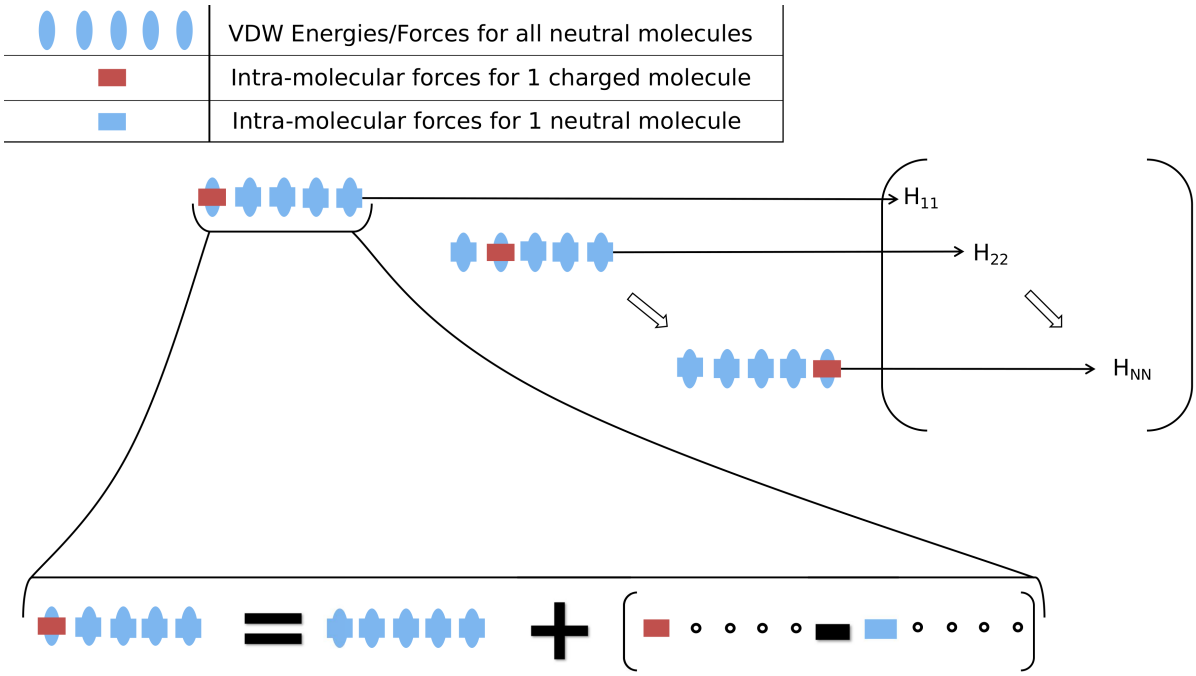

Figure 6.3: A depiction of the decomposition of the forces and energies within FOB-SH. First the all neutral VDW forces/energies are computed (blue ovals). Second the intra-molecular forces for each charged (neutral) molecule, represented by a red (blue) rectangle. The site-energy/force is then computed as a summation of all molecules in their neutral state with a molecule in its neutral state subtracted and the same molecule in its charged state added.

molecular components (bonds, bends, torsions etc…) and inter-molecular components (Van der Waals forces provided by a Leonard-Jones potential). The same repetition of the calculation of forces and energies would, at first glance, be required for the correct calculation of these terms. However, an addition-subtraction scheme is used to reduce the calculation time from $O(N_{mol},N_{atom}^2)$ to $O(N_{atom}^2)$. This is summarised in figure 6.3 and relies on the fact that the intra-molecular forces and energies can be decomposed into independent molecular contributions. In order to calculate the force on each atom and site-energy with molecule γ in its charged state the code first calculates the force/energy with all molecules in their neutral state and then adds the contribution of molecule γ in its charged state and subtracts the contribution of molecule γ in its neutral state. We do not make the same adjustment for the VDW forces as the correction is negligible. This results in just 2 calculations of all forces and total energies rather than $O(N_{mol})$ calculations. Seeing as the electrostatics are normally one of the most expensive parts of

a classical force-field it is particularly important that these are treated efficiently.

The addition subtraction scheme applied to the electrostatic interactions cannot be the same as the one used for the intra-molecular interactions as separate molecules are not independent and energies and forces cannot be decomposed into molecular contributions for each different site-energy. However, a similar trick can be used to reduce the cost of the Ewald sum. In the following work, the recalculation method references the method of looping over all molecules and recalculating energies and forces without optimisations. The addition-subtraction scheme is explained in the proceeding chapters.

6.1.2 Ewald Equations and the additional subtraction scheme

The standard Ewald summation for evaluating electrostatic energies in molecular dynamics simulation are given below:

$$\begin{aligned} E_{coul}\left(\mathbf{r}^N\right) = \frac{1}{2}\frac{1}{4\pi\varepsilon_0}\sum_{\mathbf{n}}\sum_{j}^{N_{at}}\sum_{i}^{N_{at}} q_i q_j \frac{erfc\left(\alpha\cdot|\mathbf{r}_{ij}+\mathbf{n}|\right)}{|\mathbf{r}_{ij}+\mathbf{n}|}\Theta\left(r_{cut}-|\mathbf{r}_{ij}+\mathbf{n}|\right) \\ +\frac{1}{2\pi V}\ \frac{1}{4\pi\varepsilon_0}\sum_{\mathbf{k}\neq 0}\frac{1}{|\mathbf{k}|^2}e^{-\frac{\pi^2}{\alpha^2}\frac{|\mathbf{k}|^2}{}}\ \left|\sum_{j}^{N_{at}} q_j e^{2\pi i\mathbf{k}\cdot\mathbf{R}_j}\right|^2 \\ -\frac{\alpha}{\sqrt{\pi}}\frac{1}{4\pi\varepsilon_0}\sum_j q_j^2 \\ -\frac{1}{2}\frac{1}{4\pi\varepsilon_0}\sum_{j}^{N_{at}}\sum_{i}^{N_{at}} q_i q_j \frac{erfc\left(\alpha\cdot|\mathbf{r}_{ij}|\right)}{|\mathbf{r}_{ij}|}\Theta\left(r_{cut}-|\mathbf{r}_{ij}|\right) \end{aligned} \tag{6.1}$$

In equation (6.1), the first term is the real-space sum. This sums over all periodic images ($\mathbf{n}$) and pairs of atoms i, j within a cutoff imposed by the Heaviside step function $\Theta(r_{cut}-|\mathbf{r}_{ij}+\mathbf{n}|)$. The distance between atoms is given by $\mathbf{r}_{ij}=\mathbf{r}_i-\mathbf{r}_j$, the charge on atom i is given by q_i and alpha is a convergence parameter. The factor $\frac{1}{2}$ accounts for any double counting of atoms. The second term is the most expensive part of this calculation and sums over reciprocal-space vectors $\mathbf{k}$ and atoms, j. $\mathbf{R}_j$ represents the position vector of atom j. The third term is the constant self-energy term and the fourth corrects for bonded (intra-molecular) interactions. The bonded interactions may be ignored in the real-space sum, this correction removes their effect from the reciprocal-space sum. As these 4 summations

are independent we can look at each one separately when implementing the addition-subtraction scheme, starting with the simplest -the self-energy term. Note in this section I will only discuss the energies, the forces are very similar and their equations are given in appendix ??.

6.1.3 Self-energy addition subtraction scheme

For each site-energy, γ, we must recalculate the full forces and energies with the excess charge located on molecule γ. This is demonstrated in equation (6.2). Note that for brevity I have replaced the factor $\frac{1}{4\pi\varepsilon_0}$ with η.

$$E^{\gamma}_{self} = \frac{\alpha}{\sqrt{\pi}}\eta\left[\sum_{j\notin\gamma}\left(q^n_j\right)^2 + \sum_{j\in\gamma}\left(q^c_j\right)^2\right] \tag{6.2}$$

In the above equation the Ewald self-energy correction contribution for site-energy γ is simply a sum of squared charges of molecules in their neutral state, for atoms belonging to molecules that aren't γ plus the sum of squared charges of atoms within γ. The molecule γ will have a different values due to the presence of the excess charge carrier. This is represented by the superscript n and c where q^n_j represents the charge on atom j where the force-field for the molecule it belongs to has been parameterised in it's neutral state (i.e. without an excess charge carrier). q^c_j represents the charge on atom j, where the force-field for the molecule the atom belongs to has been parameterised with an excess charge carrier localised on it (in its charged state).

For a single molecule system this value is the same for all γ and no optimisations are required, except to calculate this value once and use it for each γ. However, for a more complex system the addition subtraction scheme used is given in equation (6.3).

$$E^{\gamma}_{self} = \eta\underbrace{\frac{\alpha}{\sqrt{\pi}}\sum_{j}^{N_{at}}\left(q^n_j\right)^2}_{\text{Calculated Once}} + \underbrace{\frac{\alpha}{\sqrt{\pi}}\eta\sum_{j\in\gamma}\left[(q^c_j)^2-(q^n_j)^2\right]}_{\text{Calculated for each }\gamma} \tag{6.3}$$

In equation (6.3) we have removed the γ index from the most expensive part of the sum; this means we can calculate it once and store it. In the second term we only sum

over atoms in charged molecule γ and remove the contribution from molecule γ in its neutral state and add the contribution from molecule γ in its charged state. Seeing as the correction part of equation (6.3) is the only part repeated from each γ this reduces the cost of this calculation from $O(N_{mol}, N_{atom})$ to just $O(N_{atom})$. The same idea is used for the remaining terms in the Ewald sum.

6.1.4 Real-space addition subtraction

The real-space term is more complicated than the self-energy term, though the idea is the same. That is, the fully neutral contribution is calculated and for individual sites/molecules a correction is applied. This is shown in equation (6.4)

$$\begin{aligned} E^{\gamma}_{real} = & \frac{\eta}{2} \sum_{\mathbf{n}} \sum_{j}^{N_{at}} \sum_{i}^{N_{at}} q_i^n q_j^n \; R^{dir}(\mathbf{r}_{ij} + \mathbf{n}) \\ & + \frac{\eta}{2} \sum_{j \in \gamma, i \in \gamma} (q_j^c q_i^c - q_j^n q_i^n) \; R^{dir}(\mathbf{r}_{ij} + \mathbf{n}) \\ & + \frac{\eta}{2} \sum_{j \in \gamma, i \notin \gamma} (q_j^c - q_j^n) q_i^n \; R^{dir}(\mathbf{r}_{ij} + \mathbf{n}) \end{aligned} \tag{6.4}$$

In equation (6.4) the most expensive summation ($O(N_{atom}^2)$) is the first term. Fortunately, we can once again calculate this once and use the same value for each site-energy. This first term calculates all interactions between atoms belonging to molecules in their neutral state (neutral-neutral interactions). The next two terms show the addition-subtraction correction. The second term shows a sum over all pairs of atoms in the charged molecule, γ. In this term we subtract any neutral-neutral interactions and replace them with any charged-charged interactions. This scales as $O(N_{\text{atom per mol}})$ and is repeated N_{mol} times so the full correction scales as $O(N_{atom})$. The third term replaces any interactions of atoms on the charged molecule with its environment (neutral molecules), hence it removes neutral-neutral interactions and replaces them with charged-neutral interactions. This scales as $O(N_{\text{atom per mol}}, N_{atom})$ and is repeated N_{mol} times, resulting in an ultimate scaling of $O(N_{atom}^2)$. Therefore, this optimisation scales in the same manner as a single calculation of the Ewald interactions and any additional overheads will be minimal. For the avoidance of doubt, in equation (6.4) I have replaced the complementary error function and Heaviside step function in equation (6.1) with the term $R^{dir}(\mathbf{r}_{ij} + \mathbf{n})$.

6.1.5 Bonded corrections addition subtraction

The bonded correction terms remove electrostatic contributions to energies (and forces) for atoms that are bonded. This is because interactions are already accounted for by the intra-molecular force-field (bonds, bends, torsions etc…). These interactions occur within molecules and their contribution can be decomposed into molecular contributions. These interactions can therefore be handled in the same way as the intra-molecular addition-subtraction scheme as discussed in section 6.1.1.

6.1.6 Reciprocal-space addition subtraction

The reciprocal energies can be optimised using the addition-subtraction technique. However, the forces cannot. This is a big problem for any implementation of Ewald electrostatics within surface hopping as the electrostatic part of the Ewald sum is by far the most expensive. In fact in the same 250 molecule system as in figure 6.2 the reciprocal-space component took 88% of the calculation time. In larger systems this increases. Repeating this calculation N_{mol} times would be far too slow and would limit the surface hopping code to small systems of tens of molecules. However, the damped shifted forces technique (DSF)[109] can be used to approximate the electrostatic interactions without the reciprocal force term. For completeness I have included the addition-subtraction scheme for the reciprocal-space energies below in equation (6.5) and for the forces in appendix ??.

$$E^{\gamma}_{recip} = \frac{1}{2\pi V}\sum_{\mathbf{k}\neq 0}\frac{1}{|\mathbf{k}|^2}e^{\frac{\pi^2|\mathbf{k}|^2}{\eta^2}}\left|\sum_{j}^{N_{at}} q^n_j e^{2\pi\mathbf{k}\cdot\mathbf{R}_j} + \sum_{j\in\gamma}^{N_{at}}(q^c_j - q^n_j)e^{2\pi\mathbf{k}\cdot\mathbf{R}_j}\right|^2 \tag{6.5}$$

Once again in equation (6.5) the summation over all atoms can be calculated once and reused for each site-energy γ. This calculates all neutral-neutral interactions. The additional sum over atoms belonging to molecule γ is then repeated N_{mol} times for each site-energy γ.

6.2 Timing the electrostatics implementation

In figure 6.4 we can see the time taken for a single step of a surface hopping simulation for various lengths of a 1D Ethylene chain. We see as the chain size increases it becomes more important that electrostatic interactions are efficiently handled. For the 800

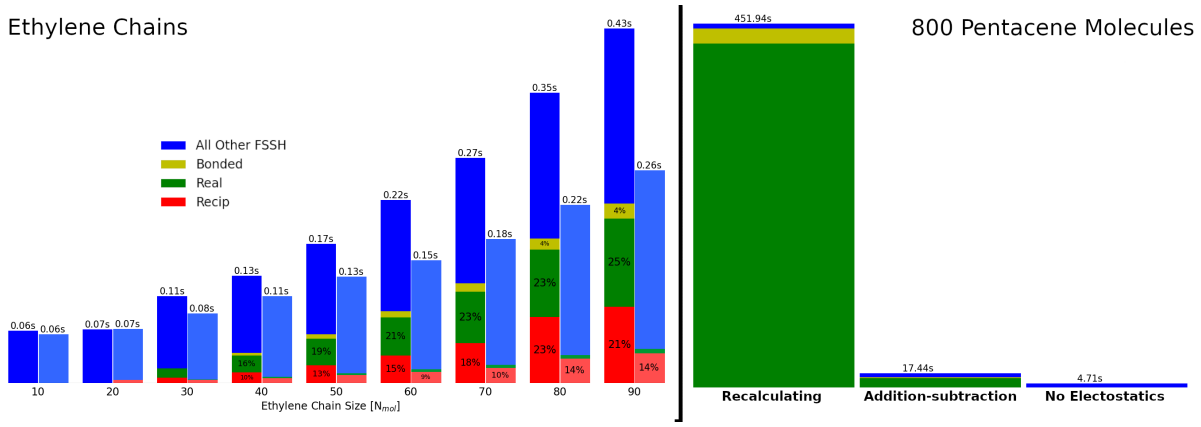

Figure 6.4: Time taken to run surface hopping and electrostatics for various lengths of 1D Ethylene chain (left) and 800 molecule pentacene plane (right). Darker colors show data from the recalculation method for the electrostatics and less saturated colors to the right show data from the addition subtraction scheme. Green bars show the time taken to calculate real-space interactions, red is reciprocal, yellow is the bonded corrections and blue shows all other parts of the surface hopping code. In the right pane reciprocal interactions are omitted as they took too long to run.

molecule pentacene plane, the reciprocal calculations were taking far too long and had to be turned off to measure the time taken for the other components. We see also that even with the addition-subtraction scheme the full reciprocal-space calculations don't see a very significant speedup. This is because the calculation of the forces are still repeated N_{mol} times as they cannot be optimised in the same way. A small speedup is seen due to the addition-subtraction scheme being used with the reciprocal-space energies. However, we see that the addition-subtraction scheme offers a major speedup for all other components. It is also vital that the results outputted are correct. I have tested both the recalculation method and the addition-subtraction method against standard CP2K calculations to ensure the implementation is correct.

6.2.1 Testing the electrostatics implementation

To test the recalculation of site-energies and forces within CP2K a 10 molecule Ethylene chain was used. In order to calculate the site-energies and forces with standard MD in CP2K, 10 different simulations were carried out. In each one of these simulations a different molecule was chosen to have charged geometry and the rest were chosen to have neutral geometry in the input files. A single step of MD was then carried out and forces and energies were outputted. These forces and energies were subsequently compared

to the forces and energies outputted by the recalculation method and the results are shown in figure 6.5 We see in figure 6.5 that the values of energy and forces as calculated

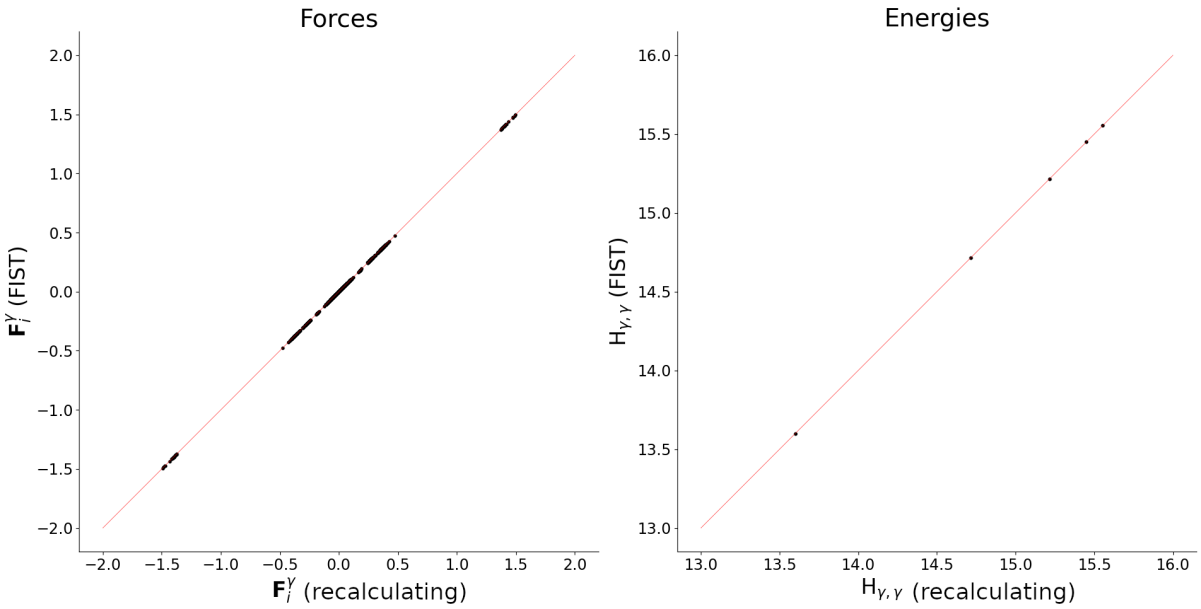

Figure 6.5: A comparison of forces and energies calculated with the recalculation method and the forces and energies calculated through multiple CP2K calculations.

with CP2K's standard MD package (FIST) and my implementation of a simple loop carrying out the same thing in the code are exactly the same. In fact the maximum absolute difference between results was 5×10^{-13} i.e. numerical error. This confirms the implementation of the recalculation scheme. The reason only 5 values for the site-energies can be seen is some points are extremely close and it is hard to see differences in them. This shows the recalculation method can now be used to benchmark the addition-subtraction scheme.

Appendix A

Tully Model Paramters

A.1 Model 1 -Single Avoided Crossing

Hamiltonian Paramters:

$$H_{11}(\mathbf{R}) = A \tanh(B\mathbf{R})$$
$$H_{12}(\mathbf{R}) = Ce^{-D\mathbf{R}^2}$$
$$H_{21}(\mathbf{R}) = H_{12}(\mathbf{R})$$
$$H_{22}(\mathbf{R}) = -H_{11}(\mathbf{R})$$

Where A = 0.03, B = 0.4, C = 0.005 and D = 0.3

Quantity	Value	Unit
Initial Position	-20	a.u.
Initial Velocities	15.0, 25.0	a.u.
Initial Adiab Pop	ground state	-
Simulation Time	6000, 4000	a.u.
$\sigma_v^{(I)}$	0.5	a.u.
M (σ constant)	40	-
$\Delta t_{\text{nuclear}}$	0.1	fs
$\Delta t_{\text{electonic}}$	0.01	fs
$\frac{\delta \mathbf{R}_{lk,v}^{(I)}}{\delta t}$ threshold	0.15	a.u.
N_{rep}	200	-

A.2 Model 2 -Dual Avoided Crossing

Hamiltonian Paramters:

$$H_{11}(\mathbf{R}) = 0$$
$$H_{12}(\mathbf{R}) = Ce^{-D\mathbf{R}^2}$$
$$H_{21}(\mathbf{R}) = H_{12}(\mathbf{R})$$
$$H_{22}(\mathbf{R}) = -Ae^{-B\mathbf{R}^2} + E$$

Where A = 0.1, B = 0.28, C = 0.015, D = 0.06 and E = 0.05

Quantity	Value	Unit
Initial Position	-8	a.u.
Initial Velocities	16.0, 30.0	a.u.
Initial Adiab Pop	ground state	-
Simulation Time	2500, 1500	a.u.
$\sigma_\nu^{(I)}$	0.5	a.u.
M (σ constant)	40	-
$\Delta t_{\text{nuclear}}$	0.1	fs
$\Delta t_{\text{electonic}}$	0.01	fs
$\frac{\delta \mathbf{R}_{lk,\nu}^{(I)}}{\delta t}$ threshold	0.15	a.u.
N_{rep}	200	-

A.3 Model 3 -Extended Coupling

Hamiltonian Paramters:

$$H_{11}(\mathbf{R}) = A$$
$$H_{12}(\mathbf{R}) = \begin{cases} Be^{C\mathbf{R}}, & R \leq 0 \\ B(2 - e^{-C\mathbf{R}}), & R > 0 \end{cases}$$
$$H_{21}(\mathbf{R}) = H_{12}(\mathbf{R})$$
$$H_{22}(\mathbf{R}) = -H_{11}(\mathbf{R})$$

Where A = 6×10^{-4}, B = 0.1 and C = 0.9

Quantity	Value	Unit
Initial Position	-15	a.u.
Initial Velocities	10, 30	a.u.
Initial Adiab Pop	ground state	-
Simulation Time	5000, 1500	a.u.
$\sigma_\nu^{(I)}$	0.5	a.u.
M (σ constant)	40	-
$\Delta t_{\text{nuclear}}$	0.1	fs
$\Delta t_{\text{electonic}}$	0.01	fs
$\frac{\delta \mathbf{R}_{lk,\nu}^{(I)}}{\delta t}$ threshold	0.15	a.u.
N_{rep}	200	-

A.4 Model 4 -Dual Arch

Hamiltonian Paramters:

$$H_{11}(\mathbf{R}) = A$$

$$H_{12}(\mathbf{R}) = \begin{cases} B\left[-e^{C(\mathbf{R}-D)} + e^{C(\mathbf{R}+D)}\right] & R \leq -D \\ B\left[e^{-C(\mathbf{R}-D)} - e^{-C(\mathbf{R}+D)}\right] & R \geq D \\ B\left[2 - e^{C(\mathbf{R}-D)} - e^{-C(\mathbf{R}+D)}\right] & -D < R < D \end{cases}$$

$$H_{21}(\mathbf{R}) = H_{12}(\mathbf{R})$$

$$H_{22}(\mathbf{R}) = -H_{11}(\mathbf{R})$$

Where A = $6\times\ 10^{-4}$, B = 0.1, C = 0.9 and D = 4

Quantity	Value	Unit
Initial Position	-20	a.u.
Initial Velocities	10, 40	a.u.
Initial Adiab Pop	ground state	-
Simulation Time	6000, 2000	a.u.
$\sigma_{\nu}^{(I)}$	0.5	a.u.
M (σ constant)	40	-
$\Delta t_{\text{nuclear}}$	0.1	fs
$\Delta t_{\text{electonic}}$	0.01	fs
$\frac{\delta \mathbf{R}_{Ik,\nu}^{(I)}}{\delta t}$ threshold	0.15	a.u.
N_{rep}	200	-

Appendix B

Wigner Distribution Derivation

The nuclear wavepacket (at time 0) is given by:

$$\chi(R) = \frac{1}{(\pi\mu^2)^{\frac{1}{4}}} e^{-\frac{(R-R_0)^2}{2\mu^2} + ik_0(R-R_0)} \tag{B.1}$$

The Wigner quassiprobability function for momentum and position (p, R) is given by:

$$W(p,R) = \frac{1}{\pi\hbar} \int_{-\infty}^{\infty} \chi^*(R+y)\chi(R-y)e^{\frac{2ipy}{\hbar}} dy \tag{B.2}$$

However, both Ehrenfest and CTMQC require atomic positions as input so we must extract the position and velocity probability densities from this. We get these from the marginal integrals of the Wigner distribution i.e.

$$|f(R)|^2 = \int_{-\infty}^{\infty} W(R,p)dp \tag{B.3}$$

$$|f(p)|^2 = \int_{-\infty}^{\infty} W(R,p)dR \tag{B.4}$$

In order to calculate these marignal integrals we must first crunch through the maths of equation (B.2). Substituting eq (B.1) into (B.2):

$$W(p,R) = \frac{1}{\pi\hbar} \int_{-\infty}^{\infty} \frac{1}{\mu\sqrt{\pi}} e^{-\frac{(R+y-R_0)^2}{2\mu^2} - 2ik_0y - \frac{(R-y-R_0)^2}{2\mu^2}} e^{\frac{2ipy}{\hbar}} dy \tag{B.5}$$

Simplifying the 2 quadratic equations (equation (B.5)) we get:

$$W(p,R) = \frac{1}{\pi\hbar}\int_{-\infty}^{\infty} \frac{1}{\mu\sqrt{\pi}} e^{-\mu^{-2}\left(y^2 - 2ik_0 y\mu^2 + (R-R_0)^2\right)} e^{\frac{2ipy}{\hbar}} dy \tag{B.6}$$

We can now take the expressions not dependant on y outside of the integral and combine the exponents.

$$W(p,R) = \frac{1}{\pi\sqrt{\pi}\mu\hbar} e^{-\frac{(R-R_0)^2}{\mu^2}} \int_{-\infty}^{\infty} e^{-\frac{y^2 + 2iy\mu^2\left(\frac{p}{\hbar} - k_0\right)}{\mu^2}} dy \tag{B.7}$$

Integrating we get:

$$\int e^{-\frac{y^2 + 2iy\mu^2\left(\frac{p}{\hbar} - k_0\right)}{\mu^2}} dy = \frac{\sqrt{\pi}\mu}{2} e^{-\frac{\mu^2}{\hbar^2}(p - \hbar k_0)^2} erf\left[\frac{y}{\mu} + i\left(\frac{p\mu}{\hbar} - \mu k_0\right)\right] \tag{B.8}$$

Applying limits we get:

$$\int_{-\infty}^{\infty} e^{-\frac{y^2 + 2iy\mu^2\left(\frac{p}{\hbar} - k_0\right)}{\mu^2}} dy = \sqrt{\pi}\mu e^{-\frac{\mu^2}{\hbar^2}(p - \hbar k_0)^2} \tag{B.9}$$

Substituting this back into the Wigner distribution (equation (B.2)) we finally get:

$$W(p,R) = \frac{1}{\pi\hbar} e^{-\frac{(R-R_0)^2}{\mu^2}} e^{-\frac{(p - \hbar k_0)^2}{\hbar^2/\mu^2}} \tag{B.10}$$

Taking the maringal integrals we get the position and velocity probability distributions:

$$|f(R)|^2 = \frac{2}{\mu\sqrt{\pi}} e^{-\frac{(R-R_0)^2}{\mu^2}} \tag{B.11}$$

$$|f(p)|^2 = \frac{2}{\frac{\hbar}{\mu}\sqrt{\pi}} e^{-\frac{\mu^2}{\hbar^2}(p - \hbar k_0)^2} \tag{B.12}$$

The above distributions are randomly sampled to get initial atomic velocities and positions for each simulation.

Appendix C

$\mathbf{R}_{lk,\nu}$ Alternatives

C.1 $\mathbf{R}_{lk,\nu}$ Extrapolation

C.2 Alternative Quantum Momentum Intercept

In Agostini, 16[2] another quantum momentum intercept term is discussed. This term is not used because, as previously discussed in section 1.4, it leads to unphysical transfer of population between adiabatic states when the nonadiabatic coupling elements are 0. However, it can be used in these Tully Models as an effective fix to the discontinuities caused by the $\mathbf{R}_{lk,\nu}$ term.

The other quantum momentum intercept, $\mathbf{R}^{(I)}_{0,\nu}$, comes directly from the construction of the nuclear density using a linear combination of a product of gaussians (see equation (1.12) in the introduction). It is defined as in equation (C.1) below:

$$\mathbf{R}^{(I)}_{0,\nu} = \sum_{J}^{N_{tr}} \left[\frac{\hbar \prod_{\nu'} g_{\sigma^{(J)}_{\nu'}(t)} \left(\mathbf{R}^{(I)}_{\nu'}(t) - \mathbf{R}^{(J)}_{\nu'}(t) \right)}{2\sigma^{(J)}_{\nu}(t)^2 \sum_{K}^{N_{tr}} \prod_{\nu'} g_{\sigma^{(K)}_{\nu'}(t)} \left(\mathbf{R}^{(I)}_{\nu'}(t) - \mathbf{R}^{K)}_{\nu'}(t) \right)} \mathbf{R}^{(I)}_{\nu} \right] \tag{C.1}$$

However, as switching to this intercept directly may cause discontinuities in itself a smoothing parameter is applied to ease the switch. This is given in equation (C.2) below:

$$[1 - A(t)] R_{good}(t) + A(t) R_{bad}(t) = R_{effective}(t) \tag{C.2}$$

R_{good} refers to the intercept that should be switched to (e.g. for the detection of a spike in the $R^{(I)}_{lk,v}$ we switch to the intercept in in equation (C.1)). $R^{(I)}_{lk,v}$ refers to the intercept that is being switched from (e.g. when it is detected that the divergence of $R^{(I)}_{lk,v}$ has finished then we switch from the alternative intercept back to $R^{(I)}_{lk,v}$). $A(t)$ is a smoothing parameter and is given in equation (C.3) below:

$$A(t) = \frac{D^{(I)}_v}{2}\left[tanh\left(t - \frac{t_{final} + t_{init}}{0.6Ndt}\right) + 1\right] \tag{C.3}$$

Where $D^{(I)}_v$ is the distance between the 2 intercepts (e.g. $D^{(I)}_v = R^{(I)}_{lk,v} - R^{(I)}_{0,v}$), N is the number of steps to take before settling solely on one intercept, t_{init} is the time of detection of the divergence, t_{final} is the time at which the code settles on 1 intercept and dt is the timestep taken.

A cartoon of this process is given in figure C.1

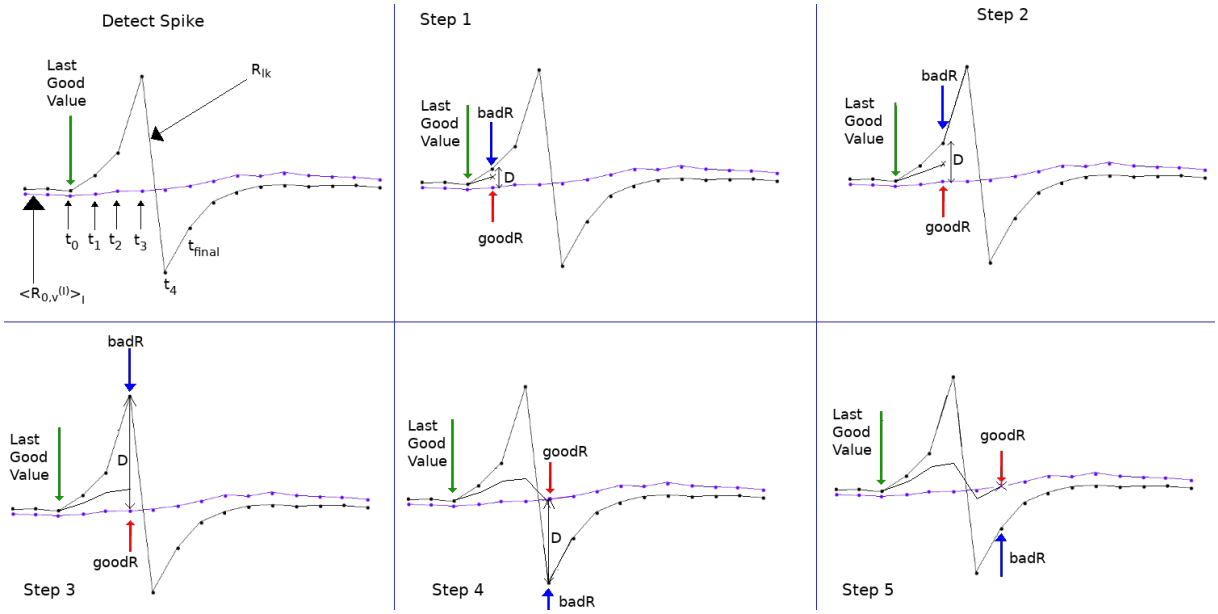

Figure C.1: A crude demonstration of the principle behind the smoothing procedure in switching between intercepts. The black line shows an intercept begin to diverge and the alternative intercept is shown in purple. As the step is incremented the amount of the alternative intercept that makes up the effective intercept is increased until only 1 intercept is used.

Appendix D

Rabi Oscillation

The time dependant Schrödinger equation is given below:

$$i\hbar\frac{\delta}{\delta t}\Phi(\mathbf{R}(t),t) = \hat{H}(\mathbf{R}(t),t)\Phi(\mathbf{R}(t),t) \tag{D.1}$$

If we hold the nuclear coordinates in place (e.g. remove time-dependence from nuclear coordinates) we get an ordinary differential equation as shown below:

$$i\hbar\frac{d}{dt}\Phi(\mathbf{R},t) = \hat{H}(\mathbf{R},t)\Phi(\mathbf{R},t) \tag{D.2}$$

This has the following general solution. This can be solved with a Taylor series expansion.

$$\Phi(\mathbf{R},t) = e^{i\hbar\hat{H}t}\Phi(\mathbf{R},0)$$

Figure

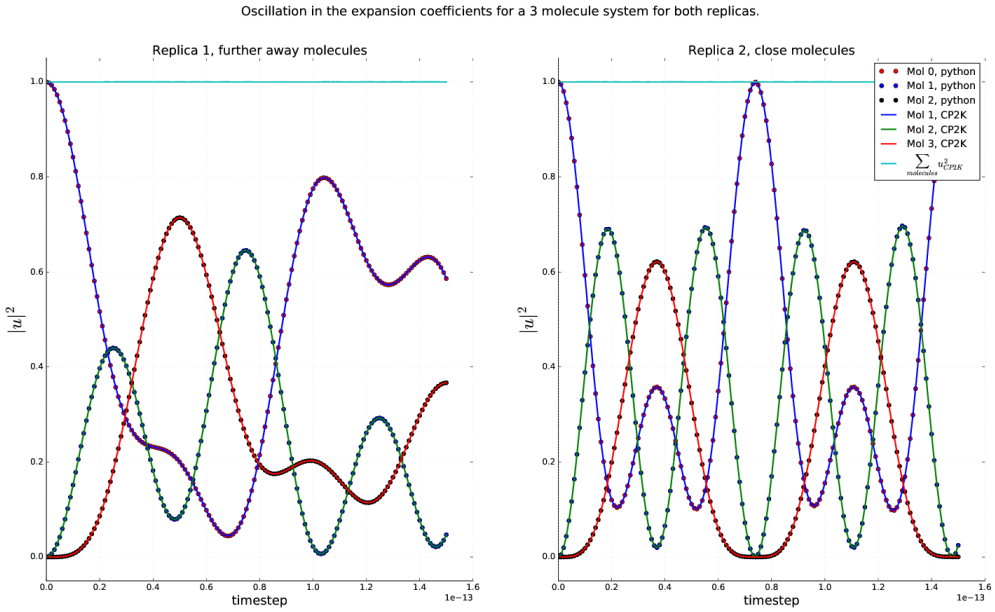

Figure D.1: Rabi oscillation occurring within a Ethylene trimer system. Dotted lines were calculated using equation (D.2), solid lines were calculated using the RK4 propagator within the CTMQC section of the CP2K code. The norm is shown on the top as a cyan line and the x axis shows the timestep in seconds.

Appendix E

Norm Conservation in CTMQC and Ehrenfest

A statement of the conservation of the norm, for a single trajectory, is given below in equation (E.1)

$$\frac{d}{dt}\sum_l |C_l(t)|^2 = \sum_l C_l^*(t)\frac{dC_l(t)}{dt} + \frac{dC_l^*(t)}{dt}C_l(t) = 2\mathbb{R}\left[\sum_l C_l(t)^*\frac{dC_l(t)}{dt}\right] \tag{E.1}$$

Substituting the equation for the evolution of the adiabatic coefficients (and removing the purely imaginary term) into (??) we get equation (E.3)

$$\frac{d}{dt}\sum_l |C_l(t)|^2 = 2\sum_l \mathbb{R}\left[\cancel{\frac{-i}{\hbar}\varepsilon^l_{BO}C_l(t)^*C_l(t)} - \sum_k \left[C_l(t)^*C_k(t)d^{ad}_{lk} - (A_l - B_l)C_l(t)^*C_l(t)\right]\right] \tag{E.2}$$

$$= -2\sum_l \mathbb{R}\left[\sum_k \left[C_l(t)^*C_k(t)d^{ad}_{lk} - (A_l - B_l)C_l(t)^*C_l(t)\right]\right] \tag{E.3}$$

Where:

$$A_l = \sum_{\nu=1}^{N_n}\sum_k \frac{\mathscr{Q}_{lk,\nu}(t)}{\hbar M_\nu}\cdot \mathbf{f}_{k,\nu}(t)|C_k(t)|^2 \tag{E.4}$$

$$B_l = \sum_{\nu=1}^{N_n}\sum_k \frac{\mathscr{Q}_{lk,\nu}(t)}{\hbar M_\nu}\cdot \mathbf{f}_{l,\nu}(t)|C_k(t)|^2 \tag{E.5}$$

The NACE term evaluates to 0 due to the anti-symmetry of the NACE giving us equation (E.7).

So far, we have proved that the norm should be conserved here for all terms apart from the quantum momentum terms i.e. Ehrenfest.

$$\frac{d}{dt}\sum_l \left|C_l^{QM}(t)\right|^2 = 2\sum_l \mathbb{R}\left[(A_l - B_l)C_l(t)^* C_l(t)\right] \tag{E.6}$$

$$= 2\left[\sum_l A_l |C_l(t)|^2 - \sum_l B_l |C_l(t)|^2\right] \tag{E.7}$$

However, $\sum_l A_l|C_l|^2 \equiv \sum_l B_l|C_l|^2$, therefore there is no change in the population and the norm should be conserved.

Appendix F

Dynamic $\boldsymbol{\sigma}$ Calculation

The algorithm for dynamically updating the σ parameter outlined in Gossel, 18[3] is provided below.

1. Set an initial width parameter $(\sigma_\nu^{(I)}(t-dt))$ and a constant we will name D.
2. Calculate a cutoff distance via: $r_{cut}(t) = D\sigma_\nu^{(I)}(t-dt)$.
3. For each atom index, ν, and replica, I, gather replicas within a cutoff distance of the current replica. Set the number of replicas within the cutoff distance to N.
4. Calculate the distance between atoms on different replicas.
5. Find the standard deviation of these distances and set the width of the gaussian, centered on atom ν and replica I, to this standard deviation.
6. If the standard deviation is smaller than $\frac{D}{N} min_I \left[\sigma_\nu^{(I)}(t-dt)\right]$ then set $\sigma_\nu^{(I)}(t) = \frac{D}{N} min_I \left[\sigma_\nu^{(I)}(t-dt)\right]$.

Appendix G

Basis Transformation

We can expand the Schrödinger equation in terms of a diabatic basis, ϕ rather than an adiabatic one, ψ. These 2 expansions are given in equations (G.1) and (G.2).

$$|\Psi\rangle = \sum_n C_n |\psi_n\rangle \tag{G.1}$$

$$|\Psi\rangle = \sum_l u_l |\phi_l\rangle \tag{G.2}$$

It follows from this we can define a transformation matrix, U_{ln} to transform between the adiabatic and diabatic bases. This is shown in equation (G.3) where the $\overleftrightarrow{I}$ symbol represents the identity matrix. This identity only holds in the orthogonal diabatic basis ϕ and wouldn't hold for non-orthogonal bases.

$$|\psi_n\rangle = \overleftrightarrow{I}\,|\psi_n\rangle = \sum_l |\phi_l\rangle\langle\phi_l|\,\psi_n\rangle = \sum_l |\phi_l\rangle U_{ln} \tag{G.3}$$

A similar relation between expansion coefficients exists

$$\sum_n C_n |\psi_n\rangle = \sum_l u_l |\phi_l\rangle \tag{G.4}$$

$$\sum_n C_n \langle\psi_m|\psi_n\rangle = \sum_l u_l \langle\psi_m|\phi_l\rangle \tag{G.5}$$

$$C_m = \sum_l u_l U^*_{lm} \tag{G.6}$$

Finally an important property of the transformation matrix is given in equation (G.7).

$$\sum_m U_{im} U^*_{lm} = \sum_m \langle \phi_i | \psi_m \rangle \langle \psi_m | \phi_l \rangle = \langle \phi_i | \phi_l \rangle = \delta_{il} \tag{G.7}$$

Equations (G.3), (G.6) and (G.7) will be used below to transform the propagation equations from the adiabatic basis to the diabatic one.

G.1 Forces

The equation for the propagation of the forces in the adiabatic basis is:

$$\begin{aligned} \mathbf{F}^{(I)}_\nu = &- \sum_n |C^{(I)}_n|^2 \nabla_\nu E^{(I)}_n - \sum_{n,m} C^{*(I)}_m C^{(I)}_n \left(E^{(I)}_n - E^{(I)}_m \right) \mathbf{d}^{ad,(I)}_{\nu,mn} \\ &- \sum_{m,n} |C^{(I)}_m|^2 \left(\sum_{\nu'}^{N_n} \frac{2}{\hbar M_{\nu'}} \mathscr{Q}^{(I)}_{\nu',mn} \cdot \mathbf{f}^{(I)}_{m,\nu'} \right) \left[\mathbf{f}^{(I)}_{n,\nu} - \mathbf{f}^{(I)}_{m,\nu} \right] |C^{(I)}_n|^2 \end{aligned} \tag{G.8}$$

The quantum momentum part of the equation cannot be easily transformed so this will focus on the Ehrenfest part:

$$\mathbf{F}^{(I)}_{eh,\nu} = - \sum_n |C^{(I)}_n|^2 \nabla_\nu E^{(I)}_n - \sum_{n,m} C^{*(I)}_m C^{(I)}_n \left(E^{(I)}_n - E^{(I)}_m \right) \mathbf{d}^{ad,(I)}_{\nu,mn} \tag{G.9}$$

Using equation (10) in Carof, 17[68] and the Hellman-Feynman theorem we can rewrite equation (G.9) as equation (G.10):

$$\mathbf{F}^{(I)}_{eh,\nu} = \sum_{m,n} C^{*(I)}_m C^{(I)}_n \langle \psi_m | \nabla_\nu H | \psi_n \rangle \tag{G.10}$$

We can substitute the coefficients and basis functions for those in equations (G.3) and (G.6). This carried out in equation (G.15). However, I have removed the trajectory and

atom index from the terms to make the notation clearer.

$$F_{eh,\nu} = \sum_{m,n} C_m^* C_n \langle \psi_m | \nabla_H | \psi_n \rangle \tag{G.11}$$

$$= \sum_{m,n} \sum_i u_i^* U_{im} \sum_j u_j U_{jn}^* \sum_l U_{lm}^* \sum_k U_{kn} \langle \phi_l | \nabla H | \phi_k \rangle \tag{G.12}$$

$$= \sum_{m,n} \sum_{i,j,k,l} u_i^* u_j U_{im} U_{lm}^* U_{jn}^* U_{kn} \langle \phi_l | \nabla H | \phi_k \rangle \tag{G.13}$$

$$= \sum_{i,j,k,l} u_i^* u_j \delta_{il} \delta_{jk} \langle \phi_l | \nabla H | \phi_k \rangle \tag{G.14}$$

$$= \sum_{i,j} u_i^* u_j \langle \phi_i | \nabla H | \phi_j \rangle \tag{G.15}$$

However, in the code the expectation value of the gradient of the Hamiltonian ($\langle \phi_i | \nabla H | \phi_j \rangle$) isn't very easily calculable. However, the gradient of the Hamiltonian matrix elements ($\nabla \langle \phi_i | H | \phi_j \rangle$) is easily calculable via the overlap term, $\nabla H = C \nabla S_{ij}$. Therefore, using chain rule we can re-write equation (G.15) as:

$$F_{eh,\nu} = \sum_{i,j} u_i^* u_j \langle \phi_i | \nabla H | \phi_j \rangle \tag{G.16}$$

$$= \sum_{i,j} u_i^* u_j \left(\nabla \langle \phi_i | H | \phi_j \rangle - \langle \nabla \phi_i | H | \phi_j \rangle - \langle \phi_i | H | \nabla \phi_j \rangle \right) \tag{G.17}$$

$$= \sum_{i,j} u_i^* u_j \left(\nabla \langle \phi_i | H | \phi_j \rangle - \sum_l \langle \nabla \phi_i | \phi_l \rangle \langle \phi_l | H | \phi_j \rangle - \sum_l \langle \phi_i | H | \phi_l \rangle \langle \phi_l | \nabla \phi_j \rangle \right) \tag{G.18}$$

$$= \sum_{i,j} u_i^* u_j \left(\nabla \langle \phi_i | H | \phi_j \rangle + \sum_l \mathbf{d}_{il} \langle \phi_l | H | \phi_j \rangle - \sum_l \mathbf{d}_{lj} \langle \phi_i | H | \phi_l \rangle \right) \tag{G.19}$$

Giving the final equation for the transformed forces as:

$$\mathbf{F}_{eh,\nu}^{(I)} = \sum_{i,j} \mathbf{u}_i^{*(I)} \mathbf{u}_j^{(I)} \left(\nabla_\nu H_{ij}^{(I)} + \sum_l \mathbf{d}_{lk,\nu}^{(I)} H_{lj}^{(I)} - \sum_l \mathbf{d}_{lj,\nu}^{(I)} H_{il} \right) \tag{G.20}$$

Appendix H

Adiabatic State Initialisation

By diagonalising the Hamiltonian we get the adiabatic energies (eigenvalues) for each state and transformation matrix (eigenvectors) to calculate diabatic states $\mathbb{U}$. We can calculate diabatic coefficients corresponding to each adiabatic state via equation (H.1) below.

$$\mathbb{U}\mathbf{C}_n = \mathbf{u}_n \tag{H.1}$$

Where $\mathbb{U}$ is the transformation matrix of size (N_{mol}, N_{mol}), $\mathbf{C}$ is a complex vector of size N_{mol} containing coefficients for adiabatic state n and $\mathbf{u}$ is a complex vector of size N_{mol} containing coefficients for diabatic state n.

Seeing as we would like to find the diabatic population corresponding to each adiabatic state we localise coefficients on each pure adiabatic state and carry out the transformation e.g: $C_i = (1+0i, 0+0i, 0+0i, ...)$ when we want to find the diabatic coefficient corresponding to state 1 and $C_i = (0+0i, 1+0i, 0+0i, ...)$ when we want to find the diabatic coefficient corresponding to state 2 etc.. Therefore, the column, n, of the transformation matrix, $\mathbb{U}$, gives the diabatic coefficients corresponding to adiabatic state, n, as shown below in equation (H.2)

$$U_{in} = u_i \tag{H.2}$$

Where n is the adiabatic state index and i is the diabatic (molecular) state index.

Once we have the diabatic state corresponding to each adiabatic state, and the en-

ergy of that adiabatic state, we can find which state best fulfills the requirements of being close to the center of the system and being within 3KT of the ground state. In order to do this, we can loop over each adiabatic state in increasing order of energy. The center of the system is calculated and the population weighted average center of mass, $\mathbf{R}_n$ of the diabatic coefficients corresponding to adiabatic state n is calculated as in equation (H.3).

$$\mathbf{R}_n = \sum_i |u_i|^2 \mathbf{R}_{COM,i} \tag{H.3}$$

The Euclidean distance between the center of the system and $\mathbf{R}_{COM,i}$ is calculated and if this distance is below some threshold value then we initialise the surface hopping trajectory on that adiabatic state. If we do not find any states within 3KT of the ground state and within an acceptable radius of the center we start again this time increasing the maximum allowed distance from the center. If this maximum allowed distance is increased such that we reach another threshold distance the energy threshold is increased this time until a state is found that is close enough to the center. In this way we find an adiabatic state, which when transformed, gives a diabatic population close to center of the system and near the ground state energy.

Appendix I

Analytic Overlap Method

Appendix J

Colophon

This is a description of the tools you used to make your thesis. It helps people make future documents, reminds you, and looks good.

(example) This document was set in the Times Roman typeface using LaTeX(specifically LuaTeX) and BibTeX, composed with Vim Used Archer, Kathleen etc...

Bibliography

[1] Federica Agostini, Ali Abedi, Yasumitsu Suzuki, Seung Kyu Min, Neepa T. Maitra, and E. K. U. Gross. The exact forces on classical nuclei in non-adiabatic charge transfer. The Journal of Chemical Physics, 142(8):084303, February 2015.

[2] Federica Agostini, Seung Kyu Min, Ali Abedi, and E. K. U. Gross. Quantum-Classical Nonadiabatic Dynamics: Coupled- vs Independent-Trajectory Methods. Journal of Chemical Theory and Computation, 12(5):2127–2143, May 2016.

[3] Graeme H. Gossel, Federica Agostini, and Neepa T. Maitra. Coupled-Trajectory Mixed Quantum-Classical Algorithm: A Deconstruction. Journal of Chemical Theory and Computation, August 2018.

[4] William Humphrey, Andrew Dalke, and Klaus Schulten. VMD – Visual Molecular Dynamics. Journal of Molecular Graphics, 14:33–38, 1996.

[5] John Stone. An Efficient Library for Parallel Ray Tracing and Animation. Master's thesis, Computer Science Department, University of Missouri-Rolla, April 1998.

[6] C. K. Chiang, C. R. Fincher, Y. W. Park, A. J. Heeger, H. Shirakawa, E. J. Louis, S. C. Gau, and Alan G. MacDiarmid. Electrical Conductivity in Doped Polyacetylene. Physical Review Letters, 39(17):1098–1101, October 1977.

[7] Hideki Shirakawa, Edwin J. Louis, Alan G. MacDiarmid, Chwan K. Chiang, and Alan J. Heeger. Synthesis of electrically conducting organic polymers: halogen derivatives of polyacetylene, (CH)x. J. Chem. Soc., Chem. Commun., 0(16):578–580, Jan 1977.

[8] Bernard Kippelen and Jean-Luc Brédas. Organic photovoltaics. Energy Environ. Sci., 2(3):251–261, 2009.

[9] M. J. Małachowski and J. Żmija. Organic field-effect transistors. Opto-Electron. Rev., 18(2):121–136, Jun 2010.

[10] N. Thejo Kalyani and S. J. Dhoble. Organic light emitting diodes: Energy saving lighting technology—A review. Renewable Sustainable Energy Rev., 16(5):2696–2723, Jun 2012.

[11] Sebastian Reineke, Frank Lindner, Gregor Schwartz, Nico Seidler, Karsten Walzer, Björn Lüssem, and Karl Leo. White organic light-emitting diodes with fluorescent tube efficiency. Nature, 459(7244):234, May 2009.

[12] Kazuki Kato, Toshihiko Iwasaki, and Takatoshi Tsujimura. Over 130 lm/w all-phosphorescent white oleds for next-generation lighting. Journal of Photopolymer Science and Technology, 28:335–340, 10 2015.

[13] Veaceslav Coropceanu, Jérôme Cornil, Demetrio A. da Silva Filho, Yoann Olivier, Robert Silbey, and Jean-Luc Brédas. Charge Transport in Organic Semiconductors. Chemical Reviews, 107(4):926–952, April 2007.

[14] Samuele Giannini, Antoine Carof, Matthew Ellis, Hui Yang, Orestis George Ziogos, Soumya Ghosh, and Jochen Blumberger. Quantum localization and delocalization of charge carriers in organic semiconducting crystals. Nature Communications, 10(1):3843, Aug 2019.

[15] Alessandro Troisi. Charge transport in high mobility molecular semiconductors: classical models and new theories. Chem. Soc. Rev., 40:2347–2358, 2011.

[16] Simone Fratini, Didier Mayou, and Sergio Ciuchi. The transient localization scenario for charge transport in crystalline organic materials. Advanced Functional Materials, 26(14):2292–2315, 2016.

[17] I. Yavuz. Dichotomy between the band and hopping transport in organic crystals: insights from experiments. Physical Chemistry Chemical Physics, 19(38):25819–25828, 2017.

[18] J. S. Brown and S. E. Shaheen. Introducing correlations into carrier transport simulations of disordered materials through seeded nucleation: impact on density of states, carrier mobility, and carrier statistics. J. Phys.: Condens. Matter, 30(13):135702, Mar 2018.

[19] Tino Zimmerling and Bertram Batlogg. Improving charge injection in high-mobility rubrene crystals: From contact-limited to channel-dominated transistors. Journal of Applied Physics, 115(16):164511, 2014.

[20] V. Podzorov, E. Menard, A. Borissov, V. Kiryukhin, J. A. Rogers, and M. E. Gershenson. Intrinsic charge transport on the surface of organic semiconductors. Phys. Rev. Lett., 93:086602, Aug 2004.

[21] Samuele Giannini, Antoine Carof, and Jochen Blumberger. Crossover from Hopping to Band-Like Charge Transport in an Organic Semiconductor Model: Atomistic Nonadiabatic Molecular Dynamics Simulation. The Journal of Physical Chemistry Letters, 9(11):3116–3123, June 2018.

[22] Harald Oberhofer, Karsten Reuter, and Jochen Blumberger. Charge Transport in Molecular Materials: An Assessment of Computational Methods. Chemical Reviews, 117(15):10319–10357, August 2017.

[23] John C. Tully. Nonadiabatic Dynamics. pages 34–71.

[24] Simone Pisana, Michele Lazzeri, Cinzia Casiraghi, Kostya S. Novoselov, A. K. Geim, Andrea C. Ferrari, and Francesco Mauri. Breakdown of the adiabatic Born–Oppenheimer approximation in graphene. Nat. Mater., 6(3):198, Feb 2007.

[25] M. Born and R. Oppenheimer. Zur Quantentheorie der Molekeln. Ann. Phys., 389(20):457–484, Jan 1927.

[26] Sharon Hammes-Schiffer. Theoretical Perspectives on Proton-Coupled Electron Transfer Reactions. Acc. Chem. Res., 34(4):273–281, Apr 2001.

[27] Sharon Hammes-Schiffer and John C. Tully. Proton transfer in solution: Molecular dynamics with quantum transitions. J. Chem. Phys., 101(6):4657–4667, Sep 1994.

[28] My Hang V. Huynh and Thomas J. Meyer. Proton-coupled electron transfer. Chemical Reviews, 107(11):5004–5064, Nov 2007.

[29] John C. Tully. Nonadiabatic molecular dynamics. International Journal of Quantum Chemistry, 40(S25):299–309, 1991.

[30] Raymond Kapral and Giovanni Ciccotti. Mixed quantum-classical dynamics. J. Chem. Phys., 110(18):8919–8929, May 1999.

[31] Todd J. Martínez∗. Insights for Light-Driven Molecular Devices from Ab Initio Multiple Spawning Excited-State Dynamics of Organic and Biological Chromophores. American Chemical Society, Oct 2005.

[32] Guillermo Albareda, Heiko Appel, Ignacio Franco, Ali Abedi, and Angel Rubio. Correlated Electron-Nuclear Dynamics with Conditional Wave Functions. Phys. Rev. Lett., 113(8):083003, Aug 2014.

[33] John C. Tully. Molecular dynamics with electronic transitions. J. Chem. Phys., 93(2):1061–1071, Jul 1990.

[34] R. L et al Whetten. Molecular dynamics beyond the adiabatic approximation: New experiments and theory. Ann. Rev. Phys. Chem., 36:277–320.

[35] Neil Shenvi, Joseph E. Subotnik, and Weitao Yang. Simultaneous-trajectory surface hopping: A parameter-free algorithm for implementing decoherence in nonadiabatic dynamics. J. Chem. Phys., 134(14):144102, Apr 2011.

[36] D. F. Coker and L. Xiao. Methods for molecular dynamics with nonadiabatic transitions. J. Chem. Phys., 102(1):496–510, Jan 1995.

[37] Joseph E. Subotnik, Amber Jain, Brian Landry, Andrew Petit, Wenjun Ouyang, and Nicole Bellonzi. Understanding the surface hopping view of electronic transitions and decoherence. Annual Review of Physical Chemistry, 67(1):387–417, 2016. PMID: 27215818.

[38] Giovanni Granucci, Maurizio Persico, and Alberto Zoccante. Including quantum decoherence in surface hopping. The Journal of Chemical Physics, 133(13):134111, 2010.

[39] Heather M. Jaeger, Sean Fischer, and Oleg V. Prezhdo. Decoherence-induced surface hopping. The Journal of Chemical Physics, 137(22):22A545, 2012.

[40] Amber Jain, Ethan Alguire, and Joseph E. Subotnik. An efficient, augmented surface hopping algorithm that includes decoherence for use in large-scale simulations. Journal of Chemical Theory and Computation, 12(11):5256–5268, Nov 2016.

[41] Joseph E. Subotnik and Neil Shenvi. A new approach to decoherence and momentum rescaling in the surface hopping algorithm. The Journal of Chemical Physics, 134(2):024105, 2011.

[42] Xiaosong Li, John C. Tully, H. Bernhard Schlegel, and Michael J. Frisch. Ab initio Ehrenfest dynamics. J. Chem. Phys., 123(8):084106, Aug 2005.

[43] Kenichiro Saita and Dmitrii V. Shalashilin. On-the-fly ab initio molecular dynamics with multiconfigurational Ehrenfest method. J. Chem. Phys., 137(22):22A506, Dec 2012.

[44] Daniela Kohen, Frank H. Stillinger, and John C. Tully. Model studies of nonadiabatic dynamics. J. Chem. Phys., 109(12):4713–4725, Sep 1998.

[45] John C. Tully. Perspective: Nonadiabatic dynamics theory. The Journal of Chemical Physics, 137(22):22A301, December 2012.

[46] Priya V. Parandekar and John C. Tully. Detailed Balance in Ehrenfest Mixed Quantum-Classical Dynamics. Journal of Chemical Theory and Computation, 2(2):229–235, March 2006.

[47] Ali Abedi, Neepa T. Maitra, and E. K. U. Gross. Exact Factorization of the Time-Dependent Electron-Nuclear Wave Function. Physical Review Letters, 105(12), September 2010.

[48] Federica Agostini, Seung Kyu Min, and E. K. U. Gross. Semiclassical analysis of the electron-nuclear coupling in electronic non-adiabatic processes. Annalen der Physik, 527(9-10):546–555, October 2015.

[49] Federica Agostini, Ali Abedi, Yasumitsu Suzuki, and E.K.U. Gross. Mixed quantum-classical dynamics on the exact time-dependent potential energy surface: a fresh look at non-adiabatic processes. Molecular Physics, 111(22-23):3625–3640, December 2013.

[50] Ali Abedi, Federica Agostini, Yasumitsu Suzuki, and E. K. U. Gross. Dynamical Steps that Bridge Piecewise Adiabatic Shapes in the Exact Time-Dependent Potential Energy Surface. Physical Review Letters, 110(26), June 2013.

[51] Seung Kyu Min, Ali Abedi, Kwang S. Kim, and E. K. U. Gross. Is the Molecular Berry Phase an Artifact of the Born-Oppenheimer Approximation? Phys. Rev. Lett., 113(26):263004, Dec 2014.

[52] Farnaz A. Shakib and Pengfei Huo. Ring Polymer Surface Hopping: Incorporating Nuclear Quantum Effects into Nonadiabatic Molecular Dynamics Simulations. J. Phys. Chem. Lett., 8(13):3073–3080, Jul 2017.

[53] Basile F. E. Curchod, Ivano Tavernelli, and Ursula Rothlisberger. Trajectory-based solution of the nonadiabatic quantum dynamics equations: an on-the-fly approach for molecular dynamics simulations. PCCP, 13(8):3231–3236, Feb 2011.

[54] Ivano Tavernelli. Ab initio–driven trajectory-based nuclear quantum dynamics in phase space. Phys. Rev. A, 87(4):042501, Apr 2013.

[55] Arne Scherrer, Federica Agostini, Daniel Sebastiani, E. K. U. Gross, and Rodolphe Vuilleumier. Nuclear velocity perturbation theory for vibrational circular dichroism:

An approach based on the exact factorization of the electron-nuclear wave function. J. Chem. Phys., 143(7):074106, Aug 2015.

[56] Seung Kyu Min, Federica Agostini, Ivano Tavernelli, and E. K. U. Gross. Ab Initio Nonadiabatic Dynamics with Coupled Trajectories: A Rigorous Approach to Quantum (De)Coherence. The Journal of Physical Chemistry Letters, 8(13):3048–3055, July 2017.

[57] John C. Tully. Molecular dynamics with electronic transitions. The Journal of Chemical Physics, 93(2):1061–1071, July 1990.

[58] Fruzsina Gajdos, Siim Valner, Felix Hoffmann, Jacob Spencer, Marian Breuer, Adam Kubas, Michel Dupuis, and Jochen Blumberger. Ultrafast Estimation of Electronic Couplings for Electron Transfer between -Conjugated Organic Molecules. Journal of Chemical Theory and Computation, 10(10):4653–4660, October 2014.

[59] J. VandeVondele, J; Hutter. Gaussian basis sets for accurate calculations on molecular systems in gas and condensed phases. The Journal of Chemical Physics, 127(11).

[60] J. Spencer, F. Gajdos, and J. Blumberger. FOB-SH: Fragment orbital-based surface hopping for charge carrier transport in organic and biological molecules and materials. The Journal of Chemical Physics, 145(6):064102, August 2016.

[61] Steven L. Fiedler and Jussi Eloranta. Nonadiabatic dynamics by mean-field and surface-hopping approaches: energy conservation considerations. Molecular Physics, 108(11):1471–1479, 2010.

[62] Joseph E. Subotnik. Augmented ehrenfest dynamics yields a rate for surface hopping. The Journal of Chemical Physics, 132(13):134112, 2010.

[63] R.B. Leighton Richard P. Feynman. The Feynman Lectures on Physics, Vol 3. Addison–Wesley, 1998.

[64] James Kirkpatrick. An approximate method for calculating transfer integrals based on the zindo hamiltonian. International Journal of Quantum Chemistry, 108(1):51–56, 2008.

[65] Harald Oberhofer and Jochen Blumberger. Revisiting electronic couplings and incoherent hopping models for electron transport in crystalline c60 at ambient temperatures. Phys. Chem. Chem. Phys., 14:13846–13852, 2012.

[66] Alessandro Troisi and Giorgio Orlandi. Hole migration in dna: a theoretical analysis of the role of structural fluctuations. The Journal of Physical Chemistry B, 106(8):2093–2101, Feb 2002.

[67] Adam Kubas, Felix Hoffmann, Alexander Heck, Harald Oberhofer, Marcus Elstner, and Jochen Blumberger. Electronic couplings for molecular charge transfer: Benchmarking cdft, fodft, and fodftb against high-level ab initio calculations. The Journal of Chemical Physics, 140(10):104105, 2014.

[68] Antoine Carof, Samuele Giannini, and Jochen Blumberger. Detailed balance, internal consistency, and energy conservation in fragment orbital-based surface hopping. The Journal of Chemical Physics, 147(21):214113, December 2017.

[69] Antoine Carof, Samuele Giannini, and Jochen Blumberger. Detailed balance, internal consistency, and energy conservation in fragment orbital-based surface hopping. The Journal of Chemical Physics, 147(21):214113, 2017.

[70] Soumya Ghosh, Samuele Giannini, Kevin Lively, and Jochen Blumberger. Nonadiabatic dynamics with quantum nuclei: simulating charge transfer with ring polymer surface hopping. Faraday Discuss., 221:501–525, 2020.

[71] Antoine Carof, Samuele Giannini, and Jochen Blumberger. How to calculate charge mobility in molecular materials from surface hopping non-adiabatic molecular dynamics – beyond the hopping/band paradigm. Phys. Chem. Chem. Phys., 21:26368–26386, 2019.

[72] J. Spencer, F. Gajdos, and J. Blumberger. Fob-sh: Fragment orbital-based surface hopping for charge carrier transport in organic and biological molecules and materials. The Journal of Chemical Physics, 145(6):064102, 2016.

[73] Jacob Spencer, Laura Scalfi, Antoine Carof, and Jochen Blumberger. Confronting surface hopping molecular dynamics with marcus theory for a molecular donor–acceptor system. Faraday Discuss., 195:215–236, 2016.

[74] Samuele Giannini, Orestis George Ziogos, Antoine Carof, Matthew Ellis, and Jochen Blumberger. Flickering polarons extending over ten nanometres mediate charge transport in high-mobility organic crystals. Advanced Theory and Simulations, 3(9):2000093, 2020.

[75] Samuele Giannini, Antoine Carof, and Jochen Blumberger. Crossover from hopping to band-like charge transport in an organic semiconductor model: Atomistic nonadiabatic molecular dynamics simulation. The Journal of Physical Chemistry Letters, 9(11):3116–3123, Jun 2018.

[76] Orestis George Ziogos, Samuele Giannini, Matthew Ellis, and Jochen Blumberger. Identifying high-mobility tetracene derivatives using a non-adiabatic molecular dynamics approach. J. Mater. Chem. C, 8:1054–1064, 2020.

[77] Fruzsina Gajdos, Siim Valner, Felix Hoffmann, Jacob Spencer, Marian Breuer, Adam Kubas, Michel Dupuis, and Jochen Blumberger. Ultrafast estimation of electronic couplings for electron transfer between π-conjugated organic molecules. Journal of Chemical Theory and Computation, 10(10):4653–4660, Oct 2014.

[78] Adam Kubas, Fruzsina Gajdos, Alexander Heck, Harald Oberhofer, Marcus Elstner, and Jochen Blumberger. Electronic couplings for molecular charge transfer: benchmarking cdft, fodft and fodftb against high-level ab initio calculations. ii. Phys. Chem. Chem. Phys., 17:14342–14354, 2015.

[79] Biswajit Ray, Aditya G. Baradwaj, Bryan W. Boudouris, and Muhammad A. Alam. Defect characterization in organic semiconductors by forward bias capacitance–voltage (fb-cv) analysis. The Journal of Physical Chemistry C, 118(31):17461–17466, Aug 2014.

[80] W. S. Hu, Y. T. Tao, Y. J. Hsu, D. H. Wei, and Y. S. Wu. Molecular orientation of

evaporated pentacene films on gold: alignment effect of self-assembled monolayer. Langmuir, 21(6):2260–2266, Mar 2005.

[81] Tatsuo Hasegawa and Jun Takeya. Organic field-effect transistors using single crystals. Science and Technology of Advanced Materials, 10(2):024314, 2009.

[82] John E. Anthony, James S. Brooks, David L. Eaton, and Sean R. Parkin. Functionalized pentacene: improved electronic properties from control of solid-state order. Journal of the American Chemical Society, 123(38):9482–9483, Sep 2001.

[83] John E. Anthony, David L. Eaton, and Sean R. Parkin. A road map to stable, soluble, easily crystallized pentacene derivatives. Organic Letters, 4(1):15–18, Jan 2002.

[84] A. D'Angelo, B. Edgar, A. P. Hurt, and M. D. Antonijević. Physico-chemical characterisation of three-component co-amorphous systems generated by a melt-quench method. Journal of Thermal Analysis and Calorimetry, 134(1):381–390, Oct 2018.

[85] Wanderlã L. Scopel, Antônio J. R. da Silva, and A. Fazzio. Amorphous hfo_2 and $hf_{1-x}si_xO$ via a melt-and-quench scheme using ab initio molecular dynamics. Phys. Rev. B, 77:172101, May 2008.

[86] Seth S. Berbano, Inseok Seo, Christian M. Bischoff, Katherine E. Schuller, and Steve W. Martin. Formation and structure of na2s+p2s5 amorphous materials prepared by melt-quenching and mechanical milling. Journal of Non-Crystalline Solids, 358(1):93 – 98, 2012.

[87] Pranav Karmwar, Kirsten Graeser, Keith C. Gordon, Clare J. Strachan, and Thomas Rades. Investigation of properties and recrystallisation behaviour of amorphous indomethacin samples prepared by different methods. International Journal of Pharmaceutics, 417(1):94 – 100, 2011. Advanced characterization techniques.

[88] Min-Jin Ko, Joel Plawsky, and Meyer Birnboim. Fabrication of cds/ag hybrid quantum dot composites using a melt/quench method. Journal of Non-Crystalline Solids, 203:211 – 216, 1996. Optical and Electrical Propertias of Glasses.

[89] Steve Plimpton. Fast parallel algorithms for short-range molecular dynamics. Journal of Computational Physics, 117(1):1 – 19, 1995.

[90] Steve Plimpton. Lammps software. http://lammps.sandia.gov, 1995. [Online; accessed 21-Jan-2021].

[91] Steve Plimpton, Roy Pollock, and Mark Stevens. Particle-mesh ewald and rrespa for parallel molecular dynamics simulations. In In Proceedings of the Eighth SIAM Conference on Parallel Processing for Scientific Computing, 1997.

[92] Christopher I. Bayly, Piotr Cieplak, C, and Peter A. Kollman. A well-behaved electrostatic potential based method using charge restraints for deriving atomic charges: the resp model. The Journal of Physical Chemistry, 97(40):10269–10280, Oct 1993.

[93] M. J. Frisch, G. W. Trucks, H. B. Schlegel, G. E. Scuseria, M. A. Robb, J. R. Cheeseman, G. Scalmani, V. Barone, G. A. Petersson, H. Nakatsuji, X. Li, M. Caricato, A. V. Marenich, J. Bloino, B. G. Janesko, R. Gomperts, B. Mennucci, H. P. Hratchian, J. V. Ortiz, A. F. Izmaylov, J. L. Sonnenberg, D. Williams-Young, F. Ding, F. Lipparini, F. Egidi, J. Goings, B. Peng, A. Petrone, T. Henderson, D. Ranasinghe, V. G. Zakrzewski, J. Gao, N. Rega, G. Zheng, W. Liang, M. Hada, M. Ehara, K. Toyota, R. Fukuda, J. Hasegawa, M. Ishida, T. Nakajima, Y. Honda, O. Kitao, H. Nakai, T. Vreven, K. Throssell, J. A. Montgomery, Jr., J. E. Peralta, F. Ogliaro, M. J. Bearpark, J. J. Heyd, E. N. Brothers, K. N. Kudin, V. N. Staroverov, T. A. Keith, R. Kobayashi, J. Normand, K. Raghavachari, A. P. Rendell, J. C. Burant, S. S. Iyengar, J. Tomasi, M. Cossi, J. M. Millam, M. Klene, C. Adamo, R. Cammi, J. W. Ochterski, R. L. Martin, K. Morokuma, O. Farkas, J. B. Foresman, and D. J. Fox. Gaussian˜16 Revision C.01, 2016. Gaussian Inc. Wallingford CT.

[94] Junmei Wang, Romain M. Wolf, James W. Caldwell, Peter A. Kollman, and David A. Case. Development and testing of a general amber force field. Journal of Computational Chemistry, 25(9):1157–1174, 2004.

[95] Makoto Yoneya, Masahiro Kawasaki, and Masahiko Ando. Molecular dynamics simulations of pentacene thin films: The effect of surface on polymorph selection. J. Mater. Chem., 20:10397–10402, 2010.

[96] Makoto Yoneya, Masahiro Kawasaki, and Masahiko Ando. Are pentacene monolayer and thin-film polymorphs really substrate-induced? a molecular dynamics simulation study. The Journal of Physical Chemistry C, 116(1):791–795, Jan 2012.

[97] Makoto Yoneya. Simulation of crystallization of pentacene and its derivatives from solution. The Journal of Physical Chemistry C, Jan 2021.

[98] Ryan A. Miller, Amanda Larson, and Karsten Pohl. Novel surface diffusion characteristics for a robust pentacene derivative on au(111) surfaces. Chemical Physics Letters, 678:28 – 34, 2017.

[99] Dong Wang, Ling Tang, Mengqiu Long, and Zhigang Shuai. Anisotropic thermal transport in organic molecular crystals from nonequilibrium molecular dynamics simulations. The Journal of Physical Chemistry C, 115(13):5940–5946, Apr 2011.

[100] Florian Steiner, Carl Poelking, Dorota Niedzialek, Denis Andrienko, and Jenny Nelson. Influence of orientation mismatch on charge transport across grain boundaries in tri-isopropylsilylethynyl (tips) pentacene thin films. Phys. Chem. Chem. Phys., 19:10854–10862, 2017.

[101] Ida Bagus Hendra Prastiawan, Jingxiang Xu, Yusuke Ootani, Yuji Higuchi, Nobuki Ozawa, Shingo Maruyama, Yuji Matsumoto, and Momoji Kubo. Molecular interactions between pentacene and imidazolium ionic liquids: A molecular dynamics study. Chemistry Letters, 47(9):1154–1157, 2018.

[102] EPA DSSTox. Epa dsstox. https://comptox.epa.gov/dashboard/DTXSID7059648, 2021. [Online; accessed 25-Jan-2021].

[103] Stefan Schiefer, Martin Huth, Alexander Dobrinevski, and Bert Nickel. Determination of the crystal structure of substrate-induced pentacene polymorphs

in fiber structured thin films. Journal of the American Chemical Society, 129(34):10316–10317, Aug 2007.

[104] Martin Ester, Hans-Peter Kriegel, Jörg Sander, and Xiaowei Xu. A density-based algorithm for discovering clusters in large spatial databases with noise. pages 226–231. AAAI Press, 1996.

[105] John C. Tully. Molecular dynamics with electronic transitions. The Journal of Chemical Physics, 93(2):1061–1071, 1990.

[106] P. P. Ewald. Die berechnung optischer und elektrostatischer gitterpotentiale. Annalen der Physik, 369(3):253–287, 1921.

[107] D. Wolf, P. Keblinski, S. R. Phillpot, and J. Eggebrecht. Exact method for the simulation of coulombic systems by spherically truncated, pairwise r−1 summation. The Journal of Chemical Physics, 110(17):8254–8282, 1999.

[108] Dirk Zahn, Bernd Schilling, and Stefan M. Kast. Enhancement of the wolf damped coulomb potential: static, dynamic, and dielectric properties of liquid water from molecular simulation. The Journal of Physical Chemistry B, 106(41):10725–10732, Oct 2002.

[109] Christopher J. Fennell and J. Daniel Gezelter. Is the ewald summation still necessary? pairwise alternatives to the accepted standard for long-range electrostatics. The Journal of Chemical Physics, 124(23):234104, 2006.